

DIMENSION REDUCTION APPLIED TO A MODEL OF SEA BREEZES

ITIR MOGULTAY, TODD F. DUPONT AND GIDON ESHEL

ABSTRACT. Dimension reduction is applied to a model of the sea breeze. A two-dimensional model which exhibits behavior commonly seen near shore lines is semi-discretized in one direction using a Galerkin method. This gives a small system of one-dimensional partial differential equations. The basis functions for the Galerkin are chosen based on the nature of the sea breeze circulation. Using two basis functions constructed from polynomials composed with an exponential gives a model with results comparable to observations. Stability and convergence results are proved for the Galerkin method on the sea breeze model.

1. INTRODUCTION

When applied to a system of partial differential equations, dimension-reduction techniques produce a new system which is defined over a smaller dimension. The resulting reduced dimension models are easier to compute with and easier to analyze. These techniques have found applications in several fluid dynamics problems [4]. One particularly nice example is a pendant drop that lengthens and eventually breaks off. While linear analysis and higher order perturbation analysis are not effective in predicting the shape of the surface near droplet breakoff [2, 6], the Eggers reduced-dimension model provided a simple and quite accurate description of this situation [5, 6]. Here, a dimension reduction based on Galerkin methods is applied to an idealized model of the sea breeze. An interesting aspect of this dimension reduction is the use of a nonlinear transformation that concentrates on the flexibility of the function spaces involved where it is needed.

The typical pattern of a sea breeze results from temperature differences around the shoreline. During the day, the land heats up faster than the sea due to the higher heat capacity of the sea. This has the effect of lowering the air pressure over the land which causes a breeze from the sea to land. This is termed a sea breeze. Aloft, a return current of air flows from the land to the sea. During this time air rises over the land, and descends over the sea. These four branches are the daytime sea breeze circulation. The opposite circulation occurs during the night due to the land cooling faster than the sea. Close to the surface is the land-breeze. The extent and the strength of the circulation depends on many things such as the land-sea temperature contrast, stability of the atmosphere, latitude, geography and topography of the coast.

⁰The work of the first two authors was supported in part by the ASC Flash Center at the University of Chicago which is funded by the U. S. Department of Energy under contract B523820. Received by the editors June 8, 2007.

Key words and phrases. dimension reduction, Galerkin reduction, sea-breeze.

To aid our understanding of sea breezes we resort to modeling. Many modelers use a two-dimensional domain [8], neglecting variations along the coastline while others use three-dimensional domains [10, 11]. Analytical studies of the sea breeze may neglect significant physical processes such as advection, friction and Coriolis force to make analysis easier. Linear models which omit the advective terms have provided valuable insight into many aspects of the sea breeze, a summary of earlier works can be found in [12]. However, there are things that the linear theory cannot predict, such as the inland propagation of the sea breeze front which is defined by an abrupt change in wind direction and intensity [7]. Linear theory shows the diurnal oscillation, but not the inertial oscillation sometimes present in the solution [8]. To include the important advection, friction, and Coriolis effect, other researchers use numerical modeling; this has its own set of problems. Sea breeze is concentrated close to the surface and close to the coast where high resolution is required, increasing computational and software effort. When the simulations are done for long periods just as in the studies of chaos [8], longer time steps are desirable. Small grids and large time steps call for the use of implicit methods, but under these conditions the numerics may over-stabilize the problem. Feliks [8] has shown that the transition to chaos for large forcing depend on the time step being used. On the other hand, the domain in which the simulations are done should be large so that the artificial boundaries have small effect on the flow near the shore, so sometimes variable grids are called for.

In spite of all the complications in simulating the sea breeze, the flows computed do not appear to be very complicated as functions of space, and this characteristic makes them reasonable candidates for dimension reduction. If it is possible to reduce the dimension of the sea breeze model, one can make numerical simulations much more easily and use higher resolution as needed. This paper takes a two-dimensional model of the sea breeze and applies dimension reduction to it, to obtain a simpler model which has many aspects of the sea breeze. The reduction is done through Galerkin reduction with several sets of basis functions. In sections (2) and (3), we present the two-dimensional model, the domain, the boundary and the initial conditions. In section (4), we present two simple Galerkin reductions. First we use Galerkin reduction using a very elementary form that illustrates the technique which does not provide realistic results. With a slightly richer space and an exponential transfer function, results are improved. We give the simulation results for the two different reduced dimension models. In sections (5) and (6), we discuss the significance of the height and length of the domain. In section (7), we introduce a general Galerkin reduction. Section (8) proves the stability of the Galerkin method using an energy estimate and section (9) proves convergence results using non-symmetric error estimates for the Galerkin method.

2. SEA BREEZE EQUATIONS

In our domain, y is distance along coastline, x is the horizontal direction perpendicular to the coastline and z is the height. We assume an infinitely long coastline and neglect variations with respect to y . The functions u , v , and w are the velocities in x -, y -, and z -directions; they are also called the zonal, meridional, and vertical velocities, respectively. We use θ for the potential temperature and ρ for the density. The variable h is the elevation perturbation of the top surface by analogy to water waves and h is a function of x only. Primes denote perturbation quantities

and the subscript m is for the mean quantities. The constant g is the gravitational constant and f is the Coriolis parameter given as $f = 2\omega \sin(\phi)$ with ω equal to the Earth's angular velocity and ϕ is the latitude. Equations for the sea breeze are [8]:

$$(2.0.1) \quad u_t + uu_x + wu_z - fv = -\frac{p_x}{\rho_m} + K_1 u_{xx} + K_2 u_{zz} - gh_x,$$

$$(2.0.2) \quad v_t + uv_x + wv_z + fu = K_1 v_{xx} + K_2 v_{zz},$$

$$(2.0.3) \quad \frac{p_z}{\rho_m} = \frac{\rho' g}{\rho_m},$$

$$(2.0.4) \quad u_x + w_z = 0,$$

$$(2.0.5) \quad \theta_t + u\theta_x + w\theta_z = K_1 \theta_{xx} + K_4 \theta_{zz},$$

$$(2.0.6) \quad -\frac{g\rho'}{\rho_m} = \frac{\theta' g}{\theta_m}.$$

The coefficients K_i 's are horizontal and vertical eddy diffusivities of momentum and heat respectively. They are large compared to the molecular diffusivity due to the presence of turbulence in the problem. In the present model, K_i 's are assumed to be constants. The values are $K_1 = 10$ and $K_2 = K_4 = 80000$ for the one-basis simulations and $K_2 = K_4 = 20000$ for the two-basis simulations. The two different simulations are described in section (4).

3. DOMAIN AND BOUNDARY CONDITIONS

The domain is $\Omega = \{(x, z) : x \in (-L, L), z \in (0, H)\}$. We will use $L = 320\text{km}$ and $H = 6\text{km}$ in our examples so that the domain is 640km long and 6km high. Here, $x = 0$ corresponds to the coastline. Values for the height and length are chosen so that the boundaries are far enough not to contaminate the solution, there will be more argument on this statement in sections (5) and (6).

The boundary conditions are such that there is no motion on the boundary, i.e. $\vec{u} = (u, v, w) = 0$ on $\partial\Omega$. On the upper boundary, the potential temperature is kept constant at $\theta_1 = 321^\circ\text{K}$, and the perturbation pressure is set to zero. At the lower boundary, θ_2 varies according to the diabatic heating:

$$(3.0.7) \quad \theta_2 = \begin{cases} 300 & x < 0, \\ 300 + \theta_0 \sin(\omega t) p_3\left(\frac{\tanh(x/L_0)}{\tanh(L/L_0)}\right) & x \geq 0, \end{cases}$$

where $p_3(x) = x^2(3 - 2x)$, $L_0 = 10\text{km}$ is a length scale and $\theta_0 = 6^\circ\text{K}$ is magnitude of the forcing. The lateral boundary conditions for the potential temperature are such that the normal derivatives vanish for θ . Initially there is no motion and the atmospheric lapse rate is 3.5°K/km with potential temperature 300°K at the surface.

4. SIMPLE GALERKIN REDUCTIONS OF THE SEA BREEZE EQUATIONS

The full equations of the sea breeze are quite complicated to solve analytically. Numerically, modelers have been faced with instability issues because the numerical solutions need high resolution close to the coast and the surface where most of the action takes place. Reduction of the equations to one-dimension will make their numerical simulations easier and higher resolution can be achieved as needed. The domain of the problem is slender, $L \gg H$. Furthermore, there is a good intuition for the vertical behavior in the system which is in the form of sea and land breezes. In each of the methods, we consider the functions u, v, w and θ are approximated by functions U, V, W and S that have a restricted form. To apply Galerkin reduction [9] to a problem, one needs a set of basis functions which depend on the type of the problem at hand. In this case, the basis functions originate from the type of behavior in the vertical direction. The zonal wind is positive(negative) in the neighborhood of the surface and negative(positive) aloft during the day(night). One can assume a reasonable behavior in the vertical and come up with reduced equations which need to be solved only for the x -direction. Therefore, it is reasonable to assume the following form for the incompressible velocity:

$$(4.0.8) \quad \begin{aligned} U(x, z, t) &= u_1(x, t)\mu_z(z) \\ W(x, z, t) &= -u_{1x}(x, t)\mu(z) \\ V(x, z, t) &= v_1(x, t)\mu_z(z), \end{aligned}$$

where $\mu(z) = \frac{z^2(z-H)^2}{4}$ and u_1, v_1 are unknown functions. It is assumed that the meridional velocity has a similar vertical behavior to the zonal velocity. The potential temperature has the simplest form satisfying the boundary conditions:

$$(4.0.9) \quad S = S_1(x, t)\nu(z) + \tilde{g}(x, z, t),$$

where $\nu(z) = z(H - z)$,

$$(4.0.10) \quad \tilde{g}(x, z, t) = (\theta_1 - \theta_2)\frac{z}{H} + \theta_2,$$

and S_1 is an unknown. Galerkin approximation is applied to the equations (2.0.1)-(2.0.6) with the above basis functions. Without going deep into details, let us give an outline of Galerkin approximation for this set of basis functions. We adopt the notation for the inner product of any Ψ and Ω as $(f, g) = \int_0^H fg dz$. Equations (2.0.1),(2.0.2) and (2.0.5) dotted with the corresponding basis functions yield that for each $x \in (-L, L)$,

$$(4.0.11) \quad \begin{aligned} (U_t, \mu_z) + (UU_x, \mu_z) + (WU_z, \mu_z) - (fV, \mu_z) = \\ \left(-\frac{P_x}{\rho_m}, \mu_z\right) + (K_1U_{xx}, \mu_z) + (K_2U_{zz}, \mu_z), \end{aligned}$$

$$(4.0.12) \quad (V_t, \mu_z) + (UV_x, \mu_z) + (WV_z, \mu_z) + (fU, \mu_z) = (K_1V_{xx}, \mu_z) + (K_2V_{zz}),$$

$$(4.0.13) \quad (S_t, \rho) + (US_x, \rho) + (WS_z, \rho) = (K_1S_{xx}, \rho) + (K_2S_{zz}, \rho),$$

where P is determined from S using (2.0.3) and (2.0.6). The h_x term vanishes because for each x , it is constant and $\mu(z)$ is zero at the top and bottom. After evaluation of the integrals and simplification, we obtain the time evolution equations for u_{1t}, v_{1t} and S_{1t} as

$$(4.0.14) \quad u_{1t} - fv_1 - \frac{3g}{2\theta_m}S_{1x} - \frac{7g}{2H^2\theta_m}\theta_{2x} - K_1u_{1xx} + \frac{42K_2}{H^2}u_1 = 0,$$

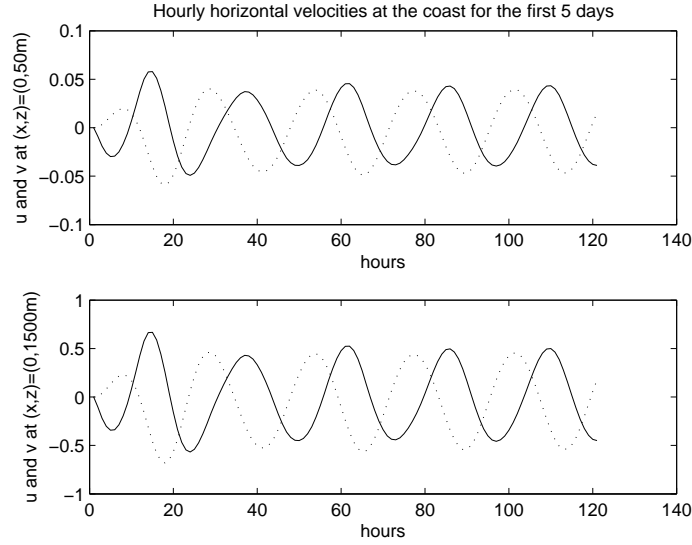


FIGURE 1. For the one-basis case, hourly horizontal velocities at the coast are plotted for 5 days. Upper panel plots the velocities at $z=50\text{m}$, and the lower panel at $z=1500\text{m}$. Solid(dotted) line corresponds to $u(v)$.

$$(4.0.15) \quad v_{1t} + fu_1 - K_1 v_{1xx} + \frac{42K_2}{H^2} v_1 = 0,$$

$$(4.0.16) \quad S_{1t} + \frac{5}{2H^2} \theta_{2t} + \frac{H}{28} u \theta_{2x} - \frac{3H}{56} u_{1x} (\theta_1 - \theta_2) - K_1 S_{1xx} - \frac{5K_1}{2H^2} \theta_{2xx} + \frac{10K_4}{H^2} S_1 = 0.$$

These equations are integrated numerically from a state of rest. Simulation results are in figures 1-2. Figure 1 plots the hourly horizontal velocities for the first 5 days. Upper(lower) panel plots the horizontal velocities at 50m(1500m) above the surface. We have chosen to plot the velocities at $z = 50\text{m}$ just to compare the results with the two basis case at the same height. Height 1500m corresponds to the approximate height where maximum sea breeze is observed with this set of basis functions. Also what is observed in figure 1 is that zonal and meridional velocities have comparable magnitudes and are 90° out of phase. Maximum sea breeze of about 0.5m/sec occurs around 8pm. In figure 2, contours of u and w are plotted corresponding to a maximum sea breeze and land breeze respectively.

This simplest one-basis case has a couple of disadvantages. Let us call the height where the zonal velocity changes its sign, the reversal height, z_r . Due to our choice, the reversal height for this one-basis case is 3km. The lateral extent of the sea breeze is about 270km inland from the shoreline as observed in figure (2). However, a typical sea breeze is mostly concentrated close to the surface and the coastline. The vertical extent of the sea breeze varies from a few hundred meters at temperate latitudes to 2km at tropics [1]. The landward penetration of the sea breeze varies with land-sea contrasts and other accompanying conditions such

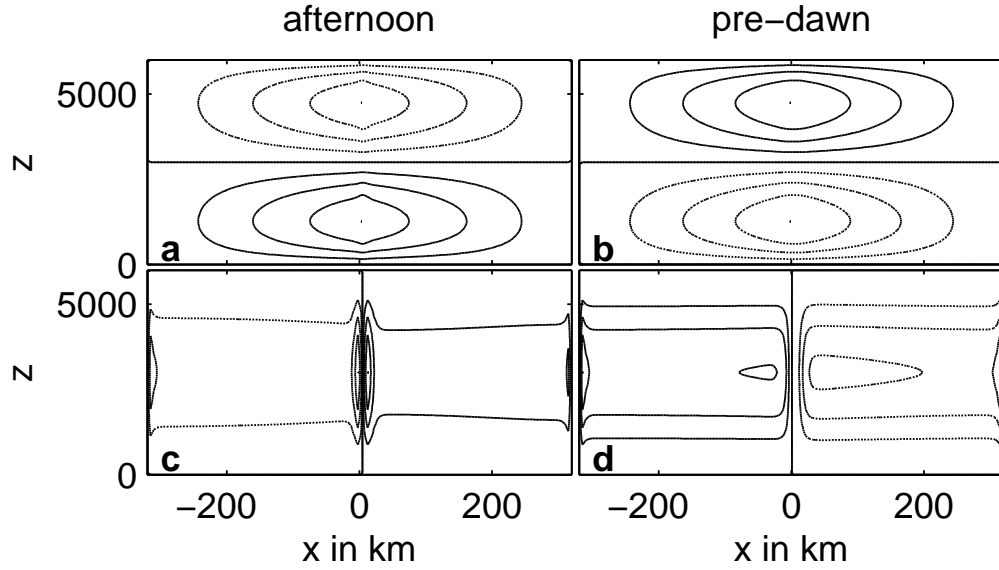


FIGURE 2. For the one-basis case, contours of the zonal velocity and vertical velocity are plotted for the maximum sea breeze and land breeze. Plot (a) is the contours of the zonal velocity and plot (c) is the contours of the vertical velocity at around 8pm when there is a maximum sea breeze. Similarly, plot (b) and (d) are the contours of u and w for the maximum land breeze. Solid(dotted) contours represent positive(negative) values. Horizontal straight lines in (a) and (b) at $z=3000\text{m}$ represent zero contour levels as well as the vertical lines at $x=0$ in (c) and (d). The absolute difference in the contour levels are approximately $(0.18,0.18)$ in plot (a), $(0.12,0.12)$ in plot (b), $(0.0016,0.0019)$ in plot (c) and $(0.0010,0.0010)$ in plot (d) where the the first(second) entry in the pairs represents the difference between the positive(negative) contour levels.

as topography and latitude. Under ideal conditions, the sea breeze is frequently observed as far as 20 – 50km from the seashore in middle latitudes [1].

The improvement to the one-basis case comes in two parts. First, we require more flexibility in the reversal height from the left boundary to the right by adding a second basis function. Second, we would like to be able to shift the reversal height in the vertical direction, especially to make it closer to the ground. In order to accomplish the two goals, we choose the basis functions as follows

$$(4.0.17) \quad U(x, z, t) = u_1(x, t)\mu_z(z) + u_2(x, t)\psi_z(z),$$

$$(4.0.18) \quad W(x, z, t) = -u_{1x}(x, t)\mu(z) - u_{2x}(x, t)\psi(z),$$

$$(4.0.19) \quad V(x, z, t) = v_1(x, t)\mu_z(z) + v_2(x, t)\psi_z(z),$$

$$(4.0.20) \quad S(x, z, t) = S_1(x, t)\rho(z) + S_2(x, t)\mu_z(z) + \tilde{g}(x, z, t),$$

where

$$(4.0.21) \quad \begin{aligned} \mu(z) &= \frac{[\phi(z)]^2[\phi(z) - H]^2}{4} \\ \rho(z) &= \phi(z)[H - \phi(z)] \\ \psi(z) &= \frac{1}{5}[\phi(z)]^2[\phi(z) - H]^2[\phi(z) - \frac{H}{2}] \\ \tilde{g}(x, z, t) &= 300 + (\theta_1 - 300)\frac{z}{H} + (\theta_2 - 300)(1 - \frac{\phi(z)}{H}), \end{aligned}$$

and

$$(4.0.22) \quad \phi(z) = \frac{H(e^{\alpha z} - 1)}{(e^{\alpha H} - 1)}.$$

Here, $\phi(z)$ is the transfer function which shifts the reversal height vertically depending on the value of α . It has fixed points 0 and H , and as α tends to 0, ϕ tends to the identity function. In case $\alpha < 0$ ($\alpha > 0$), the function shifts the reversal height to lower (higher) heights than 3km. In the following simulations, $\alpha = -0.0013$ gives us an approximate reversal height of $z_r = 525\text{m}$. The equations obtained with Galerkin approximation using the new set of basis functions are very messy and will not be given here. The 6 equations obtained are numerically integrated starting from a state of rest. The results are given in figures 3-4.

In figure 3, we have plotted the horizontal velocities at the coast for 2 different heights. The upper panel shows the velocities at $z = 50\text{m}$. When compared with figure 1 upper panel, we observe higher velocities for the two basis case at the same height. The reason is that the two basis case shifts the motion closer to the ground. The maximum horizontal velocities are observed in the vertical at about $z = 250\text{m}$ above the surface and the corresponding velocities are shown in the lower panel. We observe that the maximum sea breeze close to the surface occurs at about 2pm and that the magnitude of u is bigger compared to the magnitude of v . The maximum sea breeze at 250m is about 1.9m/sec whereas the maximum land-breeze is about 1.6m/sec. The difference between sea and land breezes is more significant in observations due to the vertical eddy diffusion coefficients being much smaller during the night. Figure 4 shows the afternoon and night contours of u and v . The reversal height is at about $z = 525\text{m}$ and the lateral extent of the sea breeze is about 30km. In figure 5, the hourly horizontal velocities are plotted in the hodograph. We observe the clockwise rotation of the sea breeze at the chosen latitude

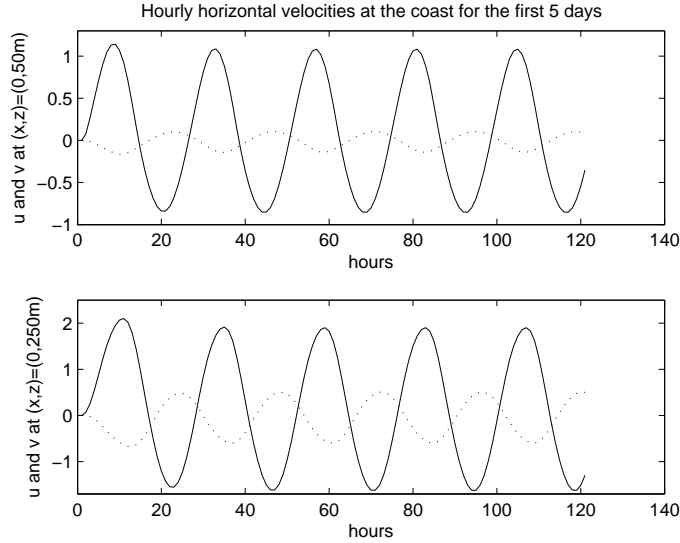


FIGURE 3. For the two-basis case, hourly horizontal velocities at the coast are plotted. Upper panel plots the velocities at $z=50\text{m}$, and the lower panel at $z=250\text{m}$. Solid(dotted) line corresponds to $u(v)$.

of 32°N . This rotation is anticlockwise in the southern hemisphere. At sunrise; the horizontal wind is in the northwest direction; i.e. there is a slight land-breeze. As the land heats up; the wind turns clockwise due to the Coriolis force. At 12pm, there is a significant sea breeze which attains its maximum at about 2pm. The sea breeze ceases between 7 and 8pm. By 12am, there is an observed land-breeze. By changing the value of α , one can get different values for the reversal height, lateral extent and the velocities.

5. SIGNIFICANCE OF THE HEIGHT OF THE DOMAIN

In section (4), we described the reversal height z_r as the height at which the zonal wind changes its sign in the vertical. From equation (4.0.22), one can solve for the approximate reversal height by setting $\phi(z)$ equal to $H/2$ as

$$(5.0.23) \quad z_r = \frac{\log(0.5e^{\alpha H} + 0.5)}{\alpha} \quad \text{for } \alpha < 0.$$

If one takes the limit of (5.0.23) as $H \rightarrow \infty$, the result is:

$$(5.0.24) \quad \lim_{H \rightarrow \infty} z_r = \frac{\log(0.5)}{\alpha}.$$

In figure 6, we have plotted the reversal height for $\alpha = -0.0013$. We see from figure 6 that at a height of approximately 5000m, the reversal height attains its asymptotic value. If we increase H from 5000m on, the circulations below and above the reversal height will not change. This is because we are not changing the diffusivities and the heating source. Therefore the horizontal and the lateral extents at which the motion takes place stay the same.

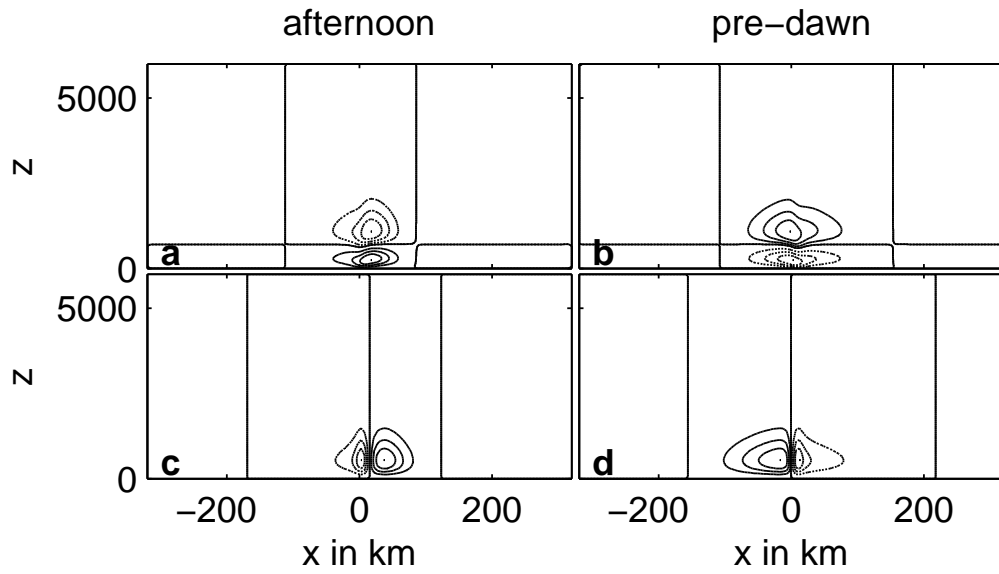


FIGURE 4. For the two-basis case, contours of the zonal velocity and vertical velocity are plotted for the maximum sea breeze and land breeze. Plot (a) is the contours of the zonal velocity and plot (c) is the contours of the vertical velocity at around 2pm when there is a maximum sea breeze. Similarly, plot (b) and (d) are the contours of u and w for the maximum land breeze. Solid(dotted) contours represent positive(negative) values. The vertical and horizontal straight lines represent zero contour levels. The absolute difference in the contour levels are approximately $(0.60, 0.24)$ in plot (a), $(0.16, 0.41)$ in plot (b), $(0.0050, 0.0062)$ in plot (c) and $(0.0022, 0.0031)$ in plot (d) where the first(second) entry in the pairs represents the difference between the positive(negative) contour levels.

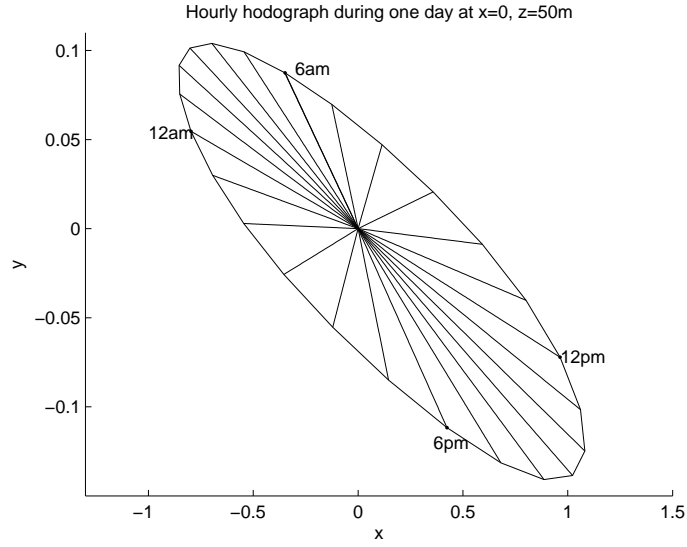


FIGURE 5. Hourly hodograph for the horizontal velocity is plotted at the coast and 50m above the surface.

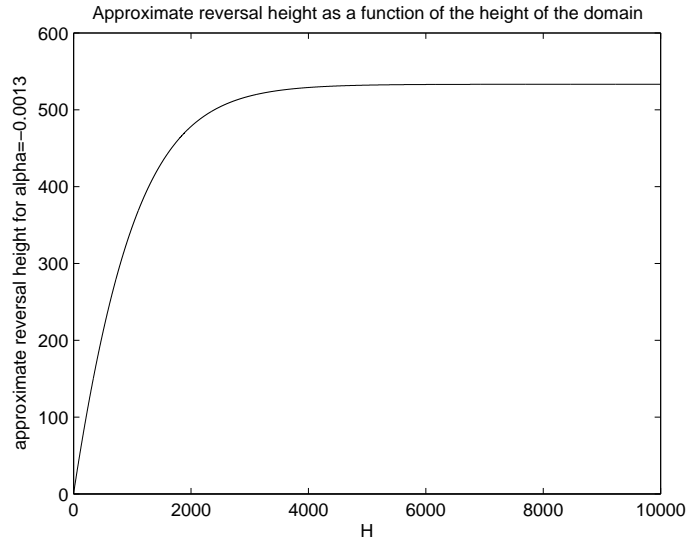


FIGURE 6. Approximate reversal height is plotted as a function of the height of the domain for $\alpha = -0.0013$.

It is worth noting that the actual height of the reversal is chosen by the reduced system and the more flexibility one includes by enriching the function spaces, the more it can deviate from (5.0.23).

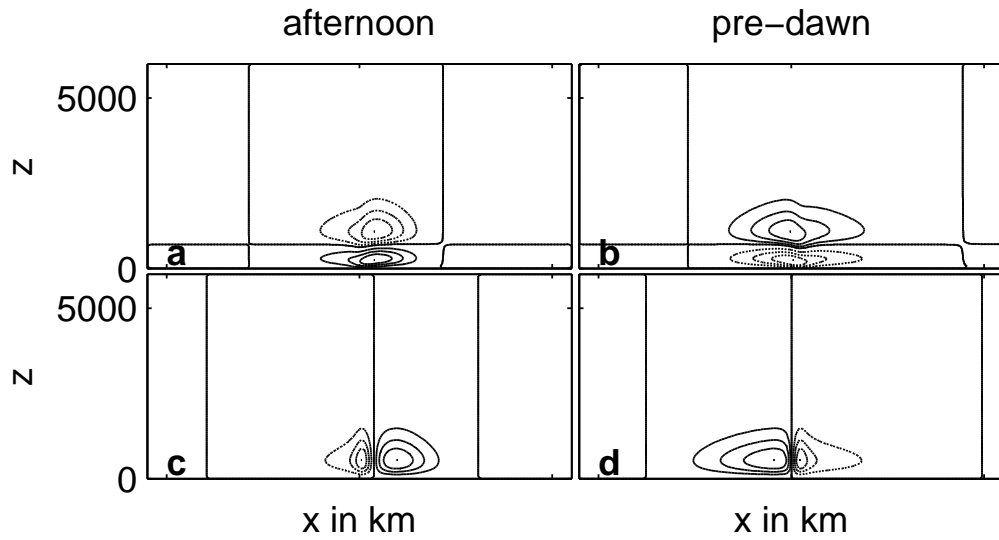


FIGURE 7. Contours of u and w corresponding to maximum sea breeze for a smaller horizontal domain of length 440km. Contour levels are the same as those given in the caption of figure 4.

6. SIGNIFICANCE OF THE LATERAL BOUNDARIES

In the introduction, we have mentioned that the domain is chosen long enough so that the lateral boundaries do not contaminate the solution. In this section, we prove our claim by plotting the solutions for a smaller and a larger length. In figures 7 and 8, we see results for a smaller ($L - 100\text{km}$) and a larger length ($L + 100\text{km}$), other parameters kept constant. What is observed is that there is no difference in the motion within the three different simulations. As the length of the domain is

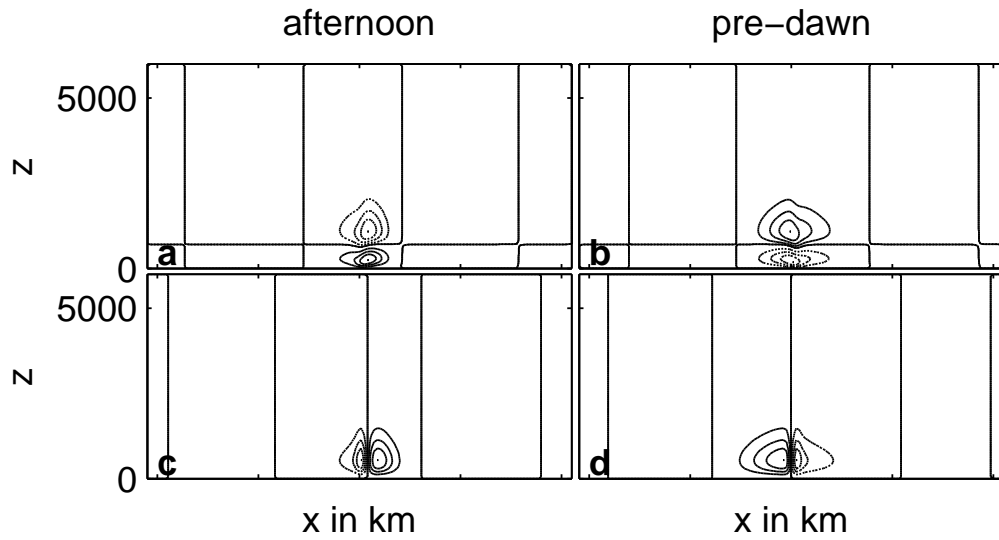


FIGURE 8. Contours of u and w corresponding to maximum sea breeze for a larger horizontal domain of length 840km. The contour levels are the same as those given in the caption of figure 4.

decreased further however, especially when the domain length is comparable to the motion's lateral extent, changes are observed. Therefore, the length of the domain being $L = 320\text{km}$ is more than sufficient to guarantee that the lateral sides do not contaminate the solution. This result has another consequence, that is the lateral boundary conditions should not affect the solution. In our problem, we have chosen vanishing velocities at the lateral sides. We have simulated the results for vanishing normal derivatives for the velocities at the lateral boundaries as well. The resulting contours are the same as in figure 4.

7. GENERAL GALERKIN REDUCTION

Suppose that $\{\mu_j\}_{j=1}^N$ is a collection of linearly independent functions in $C^3[0, H]$ such that μ_j and μ'_j both vanish at $z = 0$ and $z = H$. Also, let $\{\nu_j\}_{j=1}^M$ be a collection of C^2 functions on $[0, H]$ such that $\nu_j(0) = \nu_j(H) = 0$. Based on these functions we look for approximate solutions of the sea breeze model which generalize those given in section (4). In particular take

$$(7.0.25) \quad U(x, z, t) = \sum_{j=1}^N u_j(x, t) \mu'_j(z),$$

$$(7.0.26) \quad W(x, z, t) = - \sum_{j=1}^N \partial_x u_j(x, t) \mu_j(z),$$

$$(7.0.27) \quad V(x, z, t) = \sum_{j=1}^N v_j(x, t) \mu'_j(z),$$

$$(7.0.28) \quad S(x, z, t) = \tilde{g}(x, z, t) + \sum_{j=1}^M S_j(x, t) \nu_j(z),$$

where $\tilde{g}(x, z, t)$ is defined in (4.0.21). Notice that by construction, we have $\partial_x U + \partial_z W \equiv 0$. To define our Galerkin reduction we require for $j = 1, \dots, N$, $x \in (-L, L)$ and $t > 0$ that

$$(7.0.29) \quad (U_t + UU_x + WU_z - fV, \mu'_j) = \left(-\frac{P_x}{\rho_m} + K_1 U_{xx} + K_2 U_{zz}, \mu'_j\right),$$

$$(7.0.30) \quad (V_t + UV_x + WV_z + fU, \mu'_j) = (K_1 V_{xx} + K_2 V_{zz}, \mu'_j),$$

where $(f, g) = \int_0^H fg \, dz$. We also require for $j = 1, \dots, M$, $x \in (-L, L)$ and $t > 0$ that

$$(7.0.31) \quad (S_t + US_x + WS_z, \nu_j) = (K_1 S_{xx} + K_4 S_{zz}, \nu_j).$$

This is a system of $2N + M$ partial differential equations in x and t . We supply the boundary conditions

$$\begin{aligned} u_j(-L, t) = u_j(L, t) = 0 \quad \text{for } j = 1, \dots, N, \quad t > 0, \\ v_j(-L, t) = v_j(L, t) = 0 \quad \text{for } j = 1, \dots, N, \quad t > 0, \\ \partial_x S_j(-L, t) = \partial_x S_j(L, t) = 0 \quad \text{for } j = 1, \dots, M, \quad t > 0. \end{aligned}$$

For initial conditions, we suppose that all u_j 's, v_j 's and S_j 's are identically zero. We suppose that this system has a smooth solution. The function $P(x, z, t)$ is defined for each t by

$$(7.0.32) \quad \begin{cases} \partial_z P(x, z, t) = -\frac{\rho_m g}{\theta_m} (S(x, z, t) - \theta_m), & (x, z) \in \Omega, \\ P(x, H, t) = 0, & x \in (-L, L). \end{cases}$$

8. STABILITY OF THE GALERKIN APPROXIMATION

In this section, we give an energy argument that shows the stability of the reduced equations. This stability is the basis of the convergence results of the next section. Since these equations come from versions of the Navier-Stokes equations, it is not surprising that the energy estimate is similar to that for a parabolic equation. Specifically, we show that for $t_{final} > 0$, there is a C such that for $t \in [0, t_{final}]$,

$$(8.0.33) \quad \|U(\cdot, t)\|_{L^2(\Omega)}^2 + \|V(\cdot, t)\|_{L^2(\Omega)}^2 + \|S(\cdot, t)\|_{L^2(\Omega)}^2 \leq C.$$

In this and the next section, we use K instead of K_1 , K_2 and K_4 to simplify the notation. We also use C as a generic constant that depends on the parameters of the problem. We also will use $\|\cdot\|$ as a shorthand for $\|\cdot\|_{L^2(\Omega)}$ for scalar and vector-valued functions.

The Galerkin equations for U and V are such that we can use U and V as test functions. Thus by taking the $L^2(\Omega)$ inner product of the U and V equations with U and V respectively, we get

$$(8.0.34) \quad \frac{1}{2} \frac{d}{dt} \int_{\Omega} (U^2 + V^2) + K \int_{\Omega} (|\nabla U|^2 + |\nabla V|^2) = -\frac{1}{\rho_m} \int_{\Omega} P_x U.$$

In deriving this, we used the facts that $\int_{\Omega} (UU_x + WU_z)U = 0 = \int_{\Omega} (UV_x + WV_z)V$. Note that

$$-\frac{1}{\rho_m} \int_{\Omega} P_x U = \frac{1}{\rho_m} \int_{\Omega} P U_x = -\frac{1}{\rho_m} \int_{\Omega} P W_z = -\frac{g}{\theta_m} \int_{\Omega} S W \leq C \|S\| \|W\|.$$

We adopt the notation $S = \tilde{g} + \tilde{S}$. We cannot use S directly as a test function in the S equation since S does not vanish on the boundary. We instead proceed to develop a bound for \tilde{S} . Taking the inner product with \tilde{S} gives

$$(8.0.35) \quad \frac{1}{2} \frac{d}{dt} \int_{\Omega} \tilde{S}^2 + K \int_{\Omega} |\nabla \tilde{S}|^2 + \int_{\Omega} (U \tilde{S}_x + W \tilde{S}_z) \tilde{S} = - \int_{\Omega} (\tilde{g}_t + U \tilde{g}_x + W \tilde{g}_z) \tilde{S} - K \int_{\Omega} |\nabla \tilde{g}| |\nabla \tilde{S}|.$$

Just as in the velocity equations, the divergence-free nature of (U, W) gives that $\int_{\Omega} (U \tilde{S}_x + W \tilde{S}_z) \tilde{S} = 0 = -\frac{1}{2} \int_{\Omega} \tilde{S}^2 (U_x + W_z)$. Using the relation

$$ab \leq \epsilon a^2 + \frac{1}{4\epsilon} b^2$$

which holds for any real a and b and any positive ϵ , we get that

$$(8.0.36) \quad \frac{d}{dt} \|\tilde{S}\|^2 + K \|\nabla \tilde{S}\|^2 \leq C(\|U\| + \|W\| + 1) \|\tilde{S}\| + C,$$

where the C 's involve bounds for \tilde{g} and its derivatives in the max norm on the space-time cylinder. Combining (8.0.34) and (8.0.36), we get

$$(8.0.37) \quad \frac{d}{dt} [\|U\|^2 + \|V\|^2 + \|\tilde{S}\|^2] + K \|\nabla \tilde{S}\|^2 + 2K(\|\nabla U\|^2 + \|\nabla V\|^2) \leq C(\|U\| + \|W\| + 1) \|\tilde{S}\| + C + C\|W\| \|S\|.$$

In the right hand side of this relation, replace $\|S\|$ by $\|\tilde{S}\| + \|\tilde{g}\|$ and use the fact that $\|W\| \leq C\|W_z\| = C\|U_x\|$. It follows that

$$\begin{aligned}
 \frac{d}{dt} [\|U\|^2 + \|V\|^2 + \|\tilde{S}\|^2] &+ K\|\nabla\tilde{S}\|^2 + 2K[\|\nabla U\|^2 + \|\nabla V\|^2] \\
 &\leq C\|U\|\|\tilde{S}\| + C\|\nabla U\|\|\tilde{S}\| + C\|\tilde{S}\| + C \\
 (8.0.38) \quad &\leq K\|\nabla U\|^2 + C[\|U\|^2 + \|\tilde{S}\|^2 + 1].
 \end{aligned}$$

In this, we used that $C\|\nabla U\| \leq \frac{K}{2}\|\nabla U\|^2 + \frac{C^2}{2K}$. From the above relation, we get

$$\frac{d}{dt} [\|U\|^2 + \|V\|^2 + \|\tilde{S}\|^2] + K[\|\nabla U\|^2 + \|\nabla V\|^2 + \|\nabla\tilde{S}\|^2] \leq C(\|U\|^2 + \|\tilde{S}\|^2 + 1).$$

By Gronwall's inequality, we then get that on any interval $[0, t_{final}]$, the $L^2(\Omega)$ norms of U , V , and \tilde{S} are bounded. Then using $S = \tilde{S} + \tilde{g}$, we get the bound (8.0.33) claimed for U , V and S .

The stability argument above gives a bound in a somewhat stronger norm than explicitly claimed in (8.0.33), and since this norm appears in the convergence estimate of the next section, we will develop it here. Suppose that

$$\vartheta : J = (0, t_{final}) \rightarrow X$$

where X is equipped with a (semi)norm $\|\cdot\|_X$. If the function $\varrho(t) = \|\vartheta(t)\|_X$ is in $L^p(J)$, we use the notation

$$\|\vartheta\|_{L^p(J;X)} = \|\varrho\|_{L^p(J)}.$$

When the time interval is clear from context, we shorten this to $\|\vartheta\|_{L^p(X)}$. Let $\mathcal{N} = \text{span}(\mu'_j)_{j=1}^N$ and $\mathcal{M} = \text{span}(\nu_j)_{j=1}^M$. For any sufficiently nice function f defined on Ω define two semi-norms

$$\|f\|_{H_{\mathcal{M}}^{-1}} = \sup_{\|\nabla\sigma\|=1} \int_{\Omega} f\sigma$$

where $\sigma(x, y) = \sum_{j=1}^M \sigma_j(x)\nu_j(z)$ with $\sigma'_j(\pm L) = 0$ and

$$\|f\|_{H_{\mathcal{N}}^{-1}} = \sup_{\|\nabla\varrho\|=1} \int_{\Omega} f\varrho$$

where $\varrho(x, y) = \sum_{j=1}^N \varrho_j(x)\mu'_j(z)$ with $\varrho_j(\pm L) = 0$. Using these, define for sufficiently smooth functions $z = (z_1, z_2, z_3)$ mapping J into $H^1(\Omega)^3$, the norm

$$(8.0.40) \quad \|z\|_p^2 = \|z\|_{L^\infty(L^2(\Omega))}^2 + \|z\|_{L^2(H^1(\Omega))}^2 + \|\partial_t z_1\|_{L^p(H_{\mathcal{N}}^{-1})}^2 + \|\partial_t z_2\|_{L^p(H_{\mathcal{N}}^{-1})}^2 + \|\partial_t z_3\|_{L^p(H_{\mathcal{M}}^{-1})}^2$$

for $1 \leq p < \infty$. For the case $p = 2$, we use the short hand $\|\cdot\|$. We would prefer to deal only with $\|\cdot\|$, but weak control over W doesn't permit that. The stability argument given implies that for any $t_{final} > 0$, there is a C dependant on \tilde{g} and the parameters of the problem such that

$$\|(U, V, S)\|_{\frac{4}{3}} \leq C.$$

To see this, we need only check the bound on the semi-norms of the time derivatives since the $L^\infty(L^2(\Omega))$ and $L^2(H^1(\Omega))$ terms were done in detail. Note that if we use a test function $\sigma(x, z) = \sum_{j=1}^M \sigma_j(x)\nu_j(z)$ with $\|\sigma\|_{H^1(\Omega)} = 1$ in equation (7.0.31),

we get an expression for (S_t, σ) . All the terms are easily bounded in terms of $\|\sigma\|_{H^1(\Omega)}$ except the advection term. For that term use the following

$$\begin{aligned} \int_{\Omega} (US_x + WS_z)\sigma &= - \int_{\Omega} (U_x + W_z)S\sigma + (U\sigma_x + W\sigma_z)S \\ &= - \int_{\Omega} (U\sigma_x + W\sigma_z)S \leq (\|US\| + \|WS\|) \|\nabla\sigma\| \leq \|US\| + \|WS\|. \end{aligned}$$

We need to bound these terms in such a way that the bounds are in $L^p(J)$ for appropriate p . First,

$$\begin{aligned} \int_{\Omega} U^2 S^2 dx dz &= \int_0^H \int_{-L}^L U^2(x, z) S^2(x, z) dx dz \\ &\leq \int_0^H \left(\max_{x \in [-L, L]} S^2(x, z) \right) \left(\int_{-L}^L U^2(x, z) dx \right) dz \\ &\leq \left(\max_{z \in [0, H]} \int_{-L}^L U^2(x, z) dx \right) \int_0^H \max_{x \in [-L, L]} S^2(x, z) dz. \end{aligned}$$

For $z_o \in [0, H]$; since $U(x, 0) \equiv 0$,

$$\int_{-L}^L U^2(x, z_o) dx = \int_0^{z_o} \frac{d}{dz} \int_{-L}^L U^2(x, z) dx dz = 2 \int_0^{z_o} \int_{-L}^L UU_z(x, z) dx dz.$$

Using the fact that $U(x, H) \equiv 0$ too and adding the results we get that

$$\int_{-L}^L U^2(x, z_o) dx \leq \int_0^H \int_{-L}^L |UU_z(x, z)| dx dz \leq \|U\| \|\nabla U\|.$$

Since the bound does not depend on z_o , we can take the max norm over z_o to get

$$\max_{z \in [0, H]} \int_{-L}^L U^2(x, z) dx \leq \|U\| \|\nabla U\|.$$

The bounding of the S^2 term is a little different since it does not vanish on the left and right boundaries. For any x_o and x_1 in $[-L, L]$ and $z \in [0, H]$

$$\begin{aligned} S^2(x_o, z) &= S^2(x_1, z) + \int_{x_1}^{x_o} \partial_x (S^2(x, z)) dx \\ &\leq S^2(x_1, z) + 2 \int_{-L}^L |SS_x(x, z)| dx. \end{aligned}$$

If we integrate with respect to x_1 , we get

$$(2L)S^2(x_o, z) \leq \int_{-L}^L S^2(x, z) dx + (4L) \int_{-L}^L |SS_x(x, z)| dx.$$

Hence

$$\max_{x_o \in [-L, L]} S^2(x_o, z) \leq C \left(\int_{-L}^L S^2(x, z) dx + \int_{-L}^L |SS_x(x, z)| dx \right).$$

This implies that

$$\begin{aligned} \int_0^H \max_{x_o \in [-L, L]} S^2(x_o, z) dz &\leq C \int_{\Omega} (S^2 + |SS_x|) dx dz \\ &\leq C(\|S\|^2 + \|S\| \|\nabla S\|) \leq C\|S\| \|S\|_{H^1(\Omega)}. \end{aligned}$$

At this point, let us introduce another notation as $\|\cdot\|_1 = \|\cdot\|_{H^1(\Omega)}$. Then

$$\|US\| \leq C(\|U\|\|U\|_1\|S\|\|S\|_1)^{1/2} = C(\|U\|\|S\|)^{1/2}(\|U\|_1\|S\|_1)^{1/2}.$$

The first term in the bound is in $L^\infty(J)$ and the second is in $L^2(J)$. Hence we get that the function $\|US\|$ is in $L^2(J)$.

It would be nice if we could treat $\|WS\|$ the same way, but we do not have control of $\|W\|_1$.

$$\int_{\Omega} W^2 S^2 dx dz \leq \left(\max_{x \in [-L, L]} \int_0^H S^2(x, z) dz \right) \left(\int_{-L}^L \max_{z \in [0, H]} W^2(x, z) dx \right).$$

Since

$$\begin{aligned} \max_{z \in [0, H]} W^2(x, z) &\leq \int_0^H |WW_z| dz, \\ \int_{-L}^L \max_{z \in [0, H]} W^2(x, z) dx &\leq \|W\| \|W_z\| \leq C\|U\|_1^2. \end{aligned}$$

For $x_0, x_1 \in [-L, L]$,

$$\begin{aligned} \int_0^H S^2(x_0, z) dz &= \int_0^H S^2(x_1, z) dz + \int_{x_0}^{x_1} \frac{d}{dx} \int_0^H S^2(x, z) dz dx \\ &= \int_0^H S^2(x_1, z) dz + 2 \int_{x_1}^{x_0} \int_0^H SS_x(x, z) dz dx. \end{aligned}$$

Thus

$$\begin{aligned} \int_0^H S^2(x_0, z) dz &\leq C[\|S\|^2 + \|S\| \|S_x\|] \leq C\|S\| \|S\|_1 \\ \|WS\| &\leq \|S\|^{1/2} \|S\|_1^{1/2} \|U\|_1. \end{aligned}$$

The first term in the bound is in $L^\infty(J)$, the next is in $L^4(J)$ and the last is in $L^2(J)$. If $f \in L^4(J)$ and $g \in L^2(J)$ then for $\frac{1}{p} + \frac{1}{q} = 1$

$$\int_J |fg|^s dt \leq \left(\int_J |f|^{sp} dt \right)^{\frac{1}{p}} \left(\int_J |g|^{sq} dt \right)^{\frac{1}{q}}.$$

Take $p = 3$, $q = \frac{3}{2}$, $s = \frac{4}{3}$ and note that $sp = (3)(\frac{4}{3}) = 4$, $sq = (\frac{4}{3})(\frac{3}{2}) = 2$. This establishes the fact that there is a C such that

$$\|S_t\|_{L^{\frac{4}{3}}(H_{\mathcal{M}}^{-1})} \leq C.$$

The U_t - and V_t -terms are very similar to the S_t -term. Together these give

$$(8.0.41) \quad \|(U, V, S)\|_{\frac{4}{3}} \leq C.$$

9. CONVERGENCE OF THE GALERKIN SOLUTION

Let $\Upsilon_1 = (u, v, \theta)$ be the solution of the sea breeze model of section 2, and let $\Upsilon_2 = (U, V, S)$ be the Galerkin approximation for a given collection of functions $\{\mu'_j\}_{j=1}^N$ and $\{\nu_j\}_{j=1}^M$ as described in section 7. Take $\Upsilon_3 = (U_3, V_3, S_3)$ to be any function of the form

$$\begin{aligned} U_3(x, z, t) &= \sum_{j=1}^N U_{3,j}(x, t) \mu'_j(z) \\ V_3(x, z, t) &= \sum_{j=1}^N V_{3,j}(x, t) \mu'_j(z) \\ S_3(x, z, t) &= \tilde{g}(x, z, t) + \sum_{j=1}^M S_{3,j}(x, t) \nu_j(z) \end{aligned}$$

where the functions $U_{3,j}$, $V_{3,j}$ and $S_{3,j}$ are smooth and are such that U_3, V_3 and $S_{3,x}$ vanish at $x = \pm L$. In addition, $U_{3,j}, V_{3,j}$, and $S_{3,j}$ vanish at $t = 0$.

We will show in this section that if there is a Υ_3 that is close to Υ_1 then Υ_2 is also close to Υ_1 . That is, if the spaces $\mathcal{N} = \text{span}\{\mu'_j\}_{j=1}^N$ and $\mathcal{M} = \text{span}\{\nu_j\}_{j=1}^M$ are sufficiently rich that we can approximate the solution of the sea breeze model well, then the Galerkin solution does a good job of approximating it. As in the previous section, let $J = (0, t_{final})$. Define for $B > 0$

$$Q_B = \{\Upsilon = (\varphi_1, \varphi_2, \varphi_3) : \|\varphi_j\|_{L^\infty(\Omega \times J)} \leq B, \|\nabla \varphi_j\|_{L^\infty(\Omega \times J)} \leq B, j = 1, 2, 3\}.$$

We assume for a suitable B that $\Upsilon_1 \in Q_B$ and we require that $\Upsilon_3 \in Q_B$ as well. Here, we do not expect to use the minimum B such that $\Upsilon_1 \in Q_B$, so the constraint on Υ_3 is rather weak. The generic constants that arise in the estimates below are allowed to depend on B . The results of this section are not quite symmetric error estimates, but the use of Q_B in constraining the Υ_3 is similar to section 3.2 of [3].

We will sometimes use the notation

$$\Upsilon_i = (U_i, V_i, S_i)$$

to have a unified way of addressing the parts of these functions. We will associate to each Υ_i a W_i that is defined by (1) W_i vanishing at the bottom of the domain and (2) the pair (U_i, W_i) being divergence free in the sense that $\partial_x U_i + \partial_z W_i = 0$. We denote the pair (U_i, W_i) by \bar{U}_i when convenient. Similarly, there is a P_i for each Υ_i that is built from S_i by the relation (7.0.32). Note that if $\partial_x U_i$ is bounded so is $\partial_z W_i$, and this implies that W_i is bounded.

We adopt the addition notation

$$(9.0.42) \quad \Psi^{ij} = \Psi_i - \Psi_j,$$

for $\Psi = \Upsilon, U, V, W, S$ or P . The principle results of this section are the following:

Theorem: There is a C that depends on t_{final}, B , and the parameters of the sea breeze model, but not on \mathcal{M} and \mathcal{N} , such that

$$\|\Upsilon_1 - \Upsilon_2\|_{\frac{4}{3}} \leq C \|\Upsilon_1 - \Upsilon_3\|.$$

Corollary: The error in the reduced dimension model, $\Upsilon_1 - \Upsilon_2$, satisfies

$$\|\Upsilon_1 - \Upsilon_2\|_{\frac{4}{3}} \leq C \inf_{\Upsilon_3} \|\Upsilon_1 - \Upsilon_3\|$$

where the infimum is restricted to Υ_3 's in Q_B of the form specified above.

The corollary follows instantly from the theorem.

Proof of the Theorem: From (7.0.29) and the differential equation (2.0.1), we get that for $\varphi \in \mathcal{N}$,

$$\begin{aligned} & (U_{2t} + U_2 U_{2x} + W_2 U_{2z} - fV_2 + \frac{1}{\rho_m} P_{2x} - K(U_{2xx} + U_{2zz}), \varphi) \\ &= (U_{1t} + U_1 U_{1x} + W_1 U_{1z} - fV_1 + \frac{1}{\rho_m} P_{1x} - K(U_{1xx} + U_{1zz}), \varphi). \end{aligned}$$

Next we subtract a similar expression based on Υ_3 from each side

$$\begin{aligned} & (U_t^{23} + U_2 U_x^{23} + W_2 U_z^{23} - fV^{23} + \frac{1}{\rho_m} P_x^{23} - K(U_{xx}^{23} + U_{zz}^{23}), \varphi) \\ &= (U_t^{13} + U_1 U_{1x} - U_2 U_{3x} + W_1 U_{1z} - W_2 U_{3z} - fV^{13} + \frac{1}{\rho_m} P_x^{13} - K(U_{xx}^{13} + U_{zz}^{13}), \varphi). \end{aligned}$$

In the following, $(\cdot, \cdot)_\Omega$ will denote the $L^2(\Omega)$ inner product. Since both U_2 and U_3 are in \mathcal{N} , we can take $\varphi = U^{23}$ and integrate with respect to x . This gives

$$\begin{aligned} \frac{1}{2} \frac{d}{dt} \|U^{23}\|^2 + (\bar{U}_2 \cdot \nabla U^{23}, U^{23}) - (fV^{23}, U^{23})_\Omega + \left(\frac{1}{\rho_m} P_x^{23}, U^{23}\right)_\Omega + K \|\nabla U^{23}\|^2 = \\ (U_t^{13}, U^{23})_\Omega + (\bar{U}_1 \cdot \nabla U_1 - \bar{U}_2 \cdot \nabla U_3, U^{23})_\Omega - (fV^{13}, U^{23}) + \\ \left(\frac{1}{\rho_m} P_x^{13}, U^{23}\right)_\Omega + K(\nabla U^{13}, \nabla U^{23})_\Omega. \end{aligned}$$

Note that the term $(\bar{U}_2 \cdot \nabla U^{23}, U^{23})_\Omega$ vanishes. If we treat the equation (7.0.30) in a similar way, we get

$$\frac{1}{2} \frac{d}{dt} \|V^{23}\|^2 + (fU^{23}, V^{23})_\Omega + K \|\nabla V^{23}\|^2 =$$

$$(V_t^{13}, V^{23})_\Omega + (\bar{U}_1 \cdot \nabla V_1 - \bar{U}_2 \cdot \nabla V_3, V^{23})_\Omega + (fU^{13}, V^{23})_\Omega + K(\nabla V^{13}, \nabla V^{23})_\Omega.$$

Adding these two relations gives

$$\begin{aligned} (9.0.43) \quad \frac{1}{2} \frac{d}{dt} (\|U^{23}\|^2 + \|V^{23}\|^2) + \left(\frac{1}{\rho_m} P_x^{23}, U^{23}\right) + K(\|\nabla U^{23}\|^2 + \|\nabla V^{23}\|^2) = \\ (U_t^{13}, U^{23})_\Omega + (V_t^{13}, V^{23})_\Omega + (\bar{U}_1 \cdot \nabla U_1 - \bar{U}_2 \cdot \nabla U_3, U^{23})_\Omega + (\bar{U}_1 \cdot V_1 - \bar{U}_2 \cdot \nabla V_3, V^{23})_\Omega - \\ (fV^{13}, U^{23})_\Omega + (fU^{13}, V^{23})_\Omega + \left(\frac{1}{\rho_m} P_x^{13}, U^{23}\right) + K[(\nabla U^{13}, \nabla U^{23})_\Omega + (\nabla V^{13}, \nabla V^{23})_\Omega]. \end{aligned}$$

As in the stability argument, we will integrate the pressure terms by parts, use divergence free nature of the flow, integrate by parts again, and finally use the definition of the pressure. We get that

$$\left(\frac{1}{\rho_m} P_x^{23}, U^{23}\right)_\Omega = \left(\frac{1}{\rho_m} P^{23}, W_z^{23}\right)_\Omega = \left(-\frac{1}{\rho_m} P_z^{23}, W^{23}\right)_\Omega = \frac{g}{\theta_m} (S^{23}, W^{23})_\Omega$$

and

$$\left(\frac{1}{\rho_m} P_x^{13}, U^{23}\right)_\Omega = \frac{g}{\theta_m} (S^{13}, W^{23})_\Omega.$$

We need to manipulate the S-equation (7.0.31) in a similar way to get that for $\varphi \in \mathcal{M}$,

$$(S_t^{23} + \bar{U}_2 \cdot \nabla S^{23} - K(S_{xx}^{23} + S_{zz}^{23}), \varphi) = (S_t^{13} + \bar{U}_1 \cdot \nabla S_1 - \bar{U}_2 \cdot \nabla S_3 - K(S_{xx}^{13} + S_{zz}^{13}), \varphi).$$

Since the \tilde{g} terms cancel out, the S^{ij} terms vanish on the top and bottom. Since S_3 satisfies the zero derivative boundary conditions at $x = \pm L$, the S^{ij} terms also have the property that their derivatives vanish at $x = \pm L$. We replace φ by S^{23} and integrate with respect to x to get

$$(9.0.44) \quad \frac{1}{2} \frac{d}{dt} \|S^{23}\|^2 + K \|\nabla S^{23}\|^2 = (S_t^{13}, S^{23})_\Omega + (\bar{U}_1 \cdot \nabla S_1 - \bar{U}_2 \cdot \nabla S_3, S^{23})_\Omega + K(\nabla S^{13}, \nabla S^{23})_\Omega,$$

Again, the advective term $(\bar{U}_2 \cdot \nabla S^{23}, S^{23})$ vanishes because \bar{U}_2 is divergence free.

We have three terms of the form

$$(\bar{U}_1 \cdot \nabla \varphi_1 - \bar{U}_2 \cdot \nabla \varphi_3, \varphi^{23})$$

where $\varphi = U, V$ and S . We will illustrate the modification of this term using $\varphi = U$, but the three are treated the same way. Note that

$$\begin{aligned} \bar{U}_1 \cdot \nabla U_1 - \bar{U}_2 \cdot \nabla U_3 &= \bar{U}_1 \cdot \nabla U_1 - \bar{U}_1 \cdot \nabla U_3 + \bar{U}_1 \cdot \nabla U_3 - \bar{U}_3 \cdot \nabla U_3 + \bar{U}_3 \cdot \nabla U_3 - \bar{U}_2 \cdot \nabla U_3 \\ &= \bar{U}_1 \cdot \nabla U^{13} + \bar{U}^{13} \cdot \nabla U_3 - \bar{U}^{23} \cdot \nabla U_3. \end{aligned}$$

Since $\bar{U}_1, \nabla U_1$ and ∇U_3 are bounded,

$$\begin{aligned} |(\bar{U}_1 \cdot \nabla U_1 - \bar{U}_2 \cdot \nabla U_3, U^{23})_\Omega| &\leq \|\bar{U}_1\|_{L^\infty} \|\nabla U^{13}\| \|U^{23}\| + \|\bar{U}^{13}\| \|\nabla U_3\|_{L^\infty} \|U^{23}\| + \\ &\quad \|\bar{U}^{23}\| \|\nabla U_3\|_{L^\infty} \|U^{23}\| \leq \epsilon \|\nabla U^{23}\|^2 + C \|U^{23}\|^2 + C \|\nabla U^{13}\|^2 \end{aligned}$$

where C depends on the L^∞ bounds and on ϵ . Similarly

$$\bar{U}_1 \cdot \nabla V_1 - \bar{U}_2 \cdot \nabla V_3 = \bar{U}_1 \cdot \nabla V^{13} + \bar{U}^{13} \cdot \nabla V_3 - \bar{U}^{23} \cdot \nabla V_3.$$

So

$$\begin{aligned} |(\bar{U}_1 \cdot \nabla V_1 - \bar{U}_2 \cdot \nabla V_3, V^{23})_\Omega| &\leq \|\bar{U}_1\|_{L^\infty} \|\nabla V^{13}\| \|V^{23}\| + \|\bar{U}^{13}\| \|\nabla V_3\|_{L^\infty} \|V^{23}\| + \\ &\quad \|\bar{U}^{23}\| \|\nabla V_3\|_{L^\infty} \|V^{23}\| \leq \epsilon \|\nabla U^{23}\|^2 + C \|V^{23}\|^2 + C (\|V^{13}\|_1^2 + \|U^{13}\|_1^2). \end{aligned}$$

Also,

$$|(\bar{U}_1 \cdot \nabla S_1 - \bar{U}_2 \cdot \nabla S_3, S^{23})_\Omega| \leq \epsilon \|\nabla U^{23}\|^2 + C \|S^{23}\|^2 + C (\|S^{13}\|_1^2 + \|U^{13}\|_1^2).$$

Adding equations (9.0.43) and (9.0.44) and using the bounds obtained above yield

$$\begin{aligned} (9.0.45) \quad \frac{1}{2} \frac{d}{dt} (\|U^{23}\|^2 + \|V^{23}\|^2 + \|S^{23}\|^2) + K (\|\nabla U^{23}\|^2 + \|\nabla V^{23}\|^2 + \|\nabla S^{23}\|^2) &\leq \\ C (\|U^{23}\|^2 + \|V^{23}\|^2 + \|S^{23}\|^2) + \epsilon (\|U^{23}\|_1^2 + \|V^{23}\|_1^2 + \|S^{23}\|_1^2) + \\ C (\|U^{13}\|_1^2 + \|V^{13}\|_1^2 + \|S^{13}\|_1^2) + C (\|U_t^{13}\|_{H_N^{-1}}^2 + \|V_t^{13}\|_{H_N^{-1}}^2 + \|S_t^{13}\|_{H_M^{-1}}^2). \end{aligned}$$

Applying Gronwall inequality to (9.0.45) gives that

$$\|\Upsilon^{23}\|_{L^\infty(L^2)}^2 + \|\Upsilon^{23}\|_{L^2(H^1)}^2 \leq \|\Upsilon^{13}\|^2.$$

Next, we would like to bound the negative index semi-norms on Υ_t^{23} . We start with U_t^{23} . Take $\varphi \in H^1(\Omega)$ such that $\varphi(x, \cdot) \in \mathcal{N}$ for each x and such that φ vanishes at the left and right boundaries. In addition, we require that $\|\varphi\|_{H^1(\Omega)} = 1$. Then

$$\begin{aligned} (U_t^{23}, \varphi)_\Omega &= -(\bar{U}_2 \cdot \nabla U^{23} - fV^{23} + \frac{1}{\rho_m} P_x^{23}, \varphi)_\Omega - K(\nabla U^{23}, \nabla \varphi)_\Omega + \\ (U_t^{13} + \bar{U}_1 \cdot \nabla U_1 - \bar{U}_2 \cdot \nabla U_3 - fV^{13} + \frac{1}{\rho_m} P_x^{13}, \varphi)_\Omega + K(\nabla U^{13}, \nabla \varphi)_\Omega. \end{aligned}$$

Next note that $P_z^{ij} = -\frac{\rho_m g}{\theta_m} S^{ij}$ and $P^{ij}(x, H, z) = 0$ imply that

$$\|P_x^{ij}\| \leq C \|S_x^{ij}\|.$$

From this, we conclude that

$$\begin{aligned} (U_t^{23}, \varphi)_\Omega &\leq C [\|V^{23}\| + \|S^{23}\|_1 + \|U^{23}\|_1 + \|U_t^{13}\|_{H_N^{-1}} + \\ &\quad \|U^{13}\|_1 + \|V^{13}\| + \|S^{13}\|_1] - (\bar{U}_2 \cdot \nabla U^{23}, \varphi)_\Omega. \end{aligned}$$

The term in brackets is in $L^2(J)$, so is easy. The last term is the trouble maker, just as in the stability estimate. We can bound this term as

$$\begin{aligned} -(\bar{U}_2 \cdot \nabla U^{23}, \varphi) &= (U^{23}, \bar{U}_2 \cdot \nabla \varphi) \\ &\leq \|U^{23} U_2\| + \|U^{23} W_2\|. \end{aligned}$$

Proceeding very much as we did in section 8, we see that these terms can be bound by

$$(\|U^{23}\| \|U^{23}\|_1 \|U_2\| \|U_2\|_1)^{\frac{1}{2}} + (\|U^{23}\| \|U^{23}\|_1 \|W_2\| \|W_{2z}\|)^{\frac{1}{2}}.$$

Now,

$$\int_J \|U^{23}\| \|U^{23}\|_1 \|U_2\| \|U_2\|_1 dt \leq \|U^{23}\|_{L^\infty(L^2)} \|U_2\|_{L^\infty(L^2)} \|U^{23}\|_{L^2(H^1)} \|U_2\|_{L^2(H^1)}.$$

Hence if $q_1(t) = (\|U^{23}\| \|U^{23}\|_1 \|U_2\| \|U_2\|_1)^{\frac{1}{2}}$, we have

$$\begin{aligned} \int_J q_1^2 dt &\leq \|U^{23}\|_{L^\infty(L^2)} \|U_2\|_{L^\infty(L^2)} \int_J \|U_1^{23}\| \|U_2\|_1 dt \\ &\leq \|U^{23}\|_{L^\infty(L^2)} \|U_2\|_{L^\infty(L^2)} \|U^{23}\|_{L^2(H^1)} \|U_2\|_{L^2(H^1)} \\ &\leq C[\|U^{23}\|_{L^\infty(L^2)}^2 + \|U^{23}\|_{L^2(H^1)}^2]. \end{aligned}$$

Next we take $q_2(t) = (\|U^{23}\| \|U^{23}\|_1 \|W_2\| \|W_{2z}\|)^{\frac{1}{2}}$. The bound we have for q_2 is

$$\begin{aligned} q_2(t) &\leq (\|U^{23}\| \|U^{23}\|_1 \|U_2\|_1^2)^{\frac{1}{2}} \\ \int_J q_2^{\frac{4}{3}} dt &\leq \int_J \|U^{23}\|^{\frac{2}{3}} \|U^{23}\|_1^{\frac{2}{3}} \|U_2\|_1^{\frac{4}{3}} dt \\ &\leq \|U^{23}\|_{L^\infty(L^2)}^{\frac{2}{3}} \int_J \|U^{23}\|_1^{\frac{2}{3}} \|U_2\|_1^{\frac{4}{3}} dt \\ &\leq \|U^{23}\|_{L^\infty(L^2)}^{\frac{2}{3}} \left(\int_J (\|U^{23}\|_1^{\frac{2}{3}})^3 \right)^{\frac{1}{3}} \left(\int_J (\|U_2\|_1^{\frac{4}{3}})^{\frac{3}{2}} \right)^{\frac{2}{3}}. \end{aligned}$$

Hence

$$\begin{aligned} \|q_2\|_{L^{\frac{4}{3}}(J)} &\leq \|U^{23}\|_{L^\infty(L^2)}^{\frac{1}{2}} \|U^{23}\|_{L^2(H^1)}^{\frac{1}{2}} \|U_2\|_{L^2(H^1)} \\ &\leq C[\|U^{23}\|_{L^\infty(L^2)} + \|U^{23}\|_{L^2(H^1)}]. \end{aligned}$$

This implies that there is a C such that

$$\|U_t^{23}\|_{L^{\frac{4}{3}}(H_N^{-1})} \leq C \|\Upsilon^{13}\|.$$

The terms for V_t and S_t are a little easier since the p_x term is missing. Thus we conclude that

$$\|\Upsilon^{23}\|_{\frac{4}{3}} \leq C \|\Upsilon^{13}\|.$$

Hence

$$\|\Upsilon^{12}\|_{\frac{4}{3}} \leq \|\Upsilon^{13}\|_{\frac{4}{3}} + \|\Upsilon^{23}\|_{\frac{4}{3}} \leq \max(1, t_{final}^{\frac{1}{4}}) \|\Upsilon^{13}\| + C \|\Upsilon^{13}\|.$$

REFERENCES

1. B. W. Atkinson, *Meso-scale atmospheric circulations*, Academic Press, 1981.
2. K. C. Chaudhary and L. G. Redekopp, *The nonlinear instability of a liquid jet. part 1. theory*, J. Fluid Mech. **96** (1980), 257–274.
3. T. F. Dupont, *Mesh modification for evolution equations*, Mathematics of Computation **36** (1982), 85–107.
4. T. F. Dupont and A. E. Hosoi, *Some reduced-dimension models based on numerical methods*, Modeling and Computation for Applications in Mathematics (1998), 58–80.
5. Jens Eggers, *Drop formation-an overview, plenary lecture presented at the 75th annual gamm conference, dresden/germany, 22-26 march 2004*, Z. Angew.Math.Mech. **85** (2005), 400–410.
6. Jens Eggers and Todd F. Dupont, *Drop formation in a one-dimensional approximation of the navier-stokes equation*, J.Fluid Mech. **262** (1994), 205–221.
7. Yizhak Feliks, *A mesometeorological numerical model of the sea and land breezes involving sea-atmospheric interactions*, Contributions to Atmospheric Physics **54** (1981), no. 2, 238–257.
8. ———, *Nonlinear dynamics and chaos in the sea and land breezes*, Journal of the Atmospheric Sciences **61** (2004), no. 17, 2169–2187.

9. C. A. J. Fletcher, *Computational techniques of fluid dynamics, volume 1, fundamental and general techniques*, Springer-Verlag, 1988.
10. R.A. Pielke, *A three-dimensional numerical model of the seabreezes over south florida*, Monthly Weather Review **102** (1974), 115–139.
11. R.D.McPherson, *A numerical study of the effect of a coastal irregularity on the sea breeze*, Journal of Applied Meteorology **9** (1970), 767–777.
12. Richard Rotunno, *On the linear theory of the land and sea breeze*, Journal of the Atmospheric Sciences **40** (1983), no. 8, 1999–2009.

IMOGULTA@UCHICAGO.EDU, DEPARTMENT OF MATHEMATICS, UNIVERSITY OF CHICAGO, 5734 S. UNIVERSITY AVENUE, CHICAGO, IL 60637

DUPONT@CS.UCHICAGO.EDU, DEPARTMENT OF MATHEMATICS, UNIVERSITY OF CHICAGO, 5734 S. UNIVERSITY AVENUE, CHICAGO, IL 60637

GESHEL@SIMONS-ROCK.EDU, DIVISION OF SCIENCE, MATHEMATICS AND COMPUTING, BARD COLLEGE AT SIMON'S ROCK, 84 ALFORD RD., GREAT BARRINGTON, MA 01230